

Cite this: *Dalton Trans.*, 2018, **47**, 14277

Self-assembly of porphyrin hexamers *via* bidentate metal–ligand coordination†

Marga C. Lensen, *‡^a Roeland J. M. Nolte, ^a Alan E. Rowan, §^a
Wim Pyckhout-Hintzen, ^b Martin C. Feiters *^a and Johannes A. A. W. Elemans *^a

The supramolecular assembly of metal-porphyrin hexamers with bidentate ligands in chloroform solutions is demonstrated by UV/Vis and ¹H NMR-titrations, and Small Angle Neutron Scattering (SANS) experiments. Titrations of zinc porphyrin hexamer **Zn1** with 1,4-diazabicyclo[2,2,2]octane (DABCO) revealed that at a DABCO/**Zn1** molar ratio of 3, intermolecular sandwich complexes are formed, which can be considered as “circular-shaped porphyrin ladders”. These supramolecular complexes further aggregate into larger polymeric stacks, as a result of a combination of cooperativity effects, π–π stacking interactions, and chelate effects. The presence of rodlike assemblies in solution, formed by assembly of **Zn1** and DABCO, is confirmed by SANS-experiments. Using a model for cylindrical assemblies, curve fitting calculations reveal that rods with an average length of 26 nm and a radius of 30–35 Å were formed, corresponding to columnar stacks of approximately 30 hexamer molecules. In contrast, the metal-free hexamer **H₂1** did not form extended assemblies due to the absence of coordinative intermolecular interactions.

Received 20th April 2018,
Accepted 4th June 2018

DOI: 10.1039/c8dt01572d

rsc.li/dalton

1. Introduction

The organization of chromophoric compounds into highly ordered and well-defined assemblies is a research area with many potential applications in materials science.¹ Taking the light-harvesting systems in nature² as a blueprint, a large number of artificial chromophore arrays have been constructed *via* non-covalent interactions, with the ultimate goal to create devices that are capable of efficiently capturing light to convert it into energy. One of the approaches to construct such assemblies is *via* metal–ligand coordination. In particular, metallo-porphyrins have been employed as chromophoric building blocks, because of their ability to complex a wide variety of transition metals in their cores, which can in turn coordinate to a variety of axial ligands. As a result of the strict directional-

ity of most of these coordinative interactions, discrete porphyrin assemblies with various shapes and sizes have been developed, *e.g.* “ladders”,³ “cages”⁴ and “rings”.⁵

Cofacial connection of metal-porphyrins into so-called ‘sandwich-complexes’ is often accomplished by means of their coordination to bidentate axial ligands, such as 4,4'-bipyridine, pyrazine or DABCO (1,4-diaza[2,2,2]bicyclooctane, Fig. 1a).⁶ When zinc is used as the metal center in a porphyrin, its pentacoordinate geometry induces coordination of a bidentate axial ligand only on one face of the porphyrin, thus creating well-defined zinc porphyrin-ligand-zinc porphyrin sandwich complexes. The complexes of metal-porphyrins with DABCO can become more stable when the two porphyrin moieties are already pre-organized in a rigid conformation, *e.g.* by linking them *via* covalent or supramolecular interactions. In that case it becomes entropically more favorable for DABCO to coordinate between the two porphyrins, as a result of the chelate effect. Another way to minimize the entropy cost is to take advantage of cooperative effects that play a role in porphyrin oligomers. Anderson and co-workers were the first to demonstrate this strategy in their studies of porphyrin “ladder” complexes,³ and since then several other groups have developed similar porphyrin systems that form *via* cooperative metal–ligand coordination interactions.⁷

In earlier work our group has reported a family of cyclic porphyrin oligomers in which three,⁸ six,⁹ or twelve¹⁰ porphyrins are covalently attached to a central aromatic core. These

^aRadboud University, Institute for Molecules and Materials, Heyendaalseweg 135, 6525 AJ Nijmegen, The Netherlands. E-mail: Marga@LensenLab.de, m.feiters@science.ru.nl, j.elemans@science.ru.nl

^bJülich Centre for Neutron Science-1 & Institute for Complex Systems-1, Forschungszentrum Jülich GmbH, 52425 Jülich, Germany

† Electronic supplementary information (ESI) available. See DOI: 10.1039/c8dt01572d

‡ Present address: Technische Universität Berlin, Institut für Chemie, Nanostrukturierte Biomaterialien, Straße des 17. Juni 124, Sekr. TC 1, 10623 Berlin, Germany.

§ Present address: Australian Institute for Bioengineering and Nanotechnology (AIBN), The University of Queensland, Brisbane, QLD 4072, Australia.

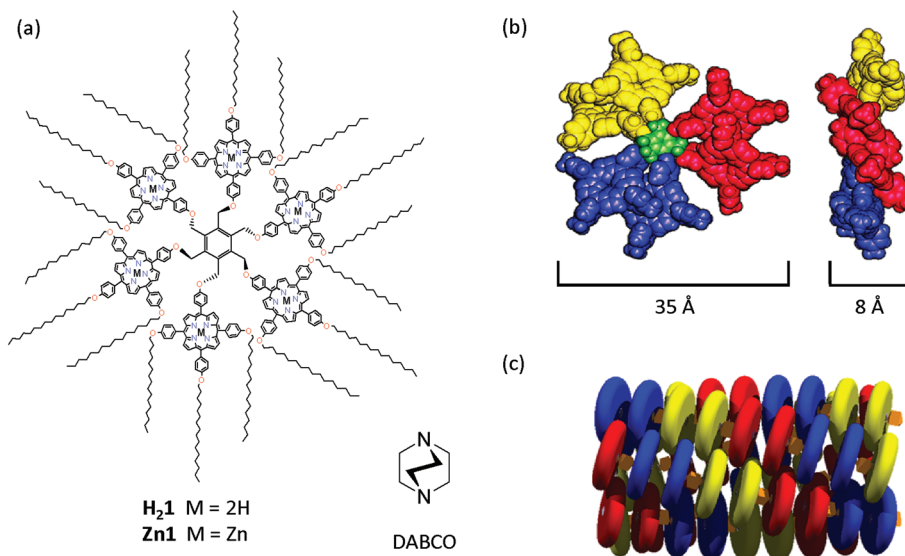


Fig. 1 (a) Structure of porphyrin hexamers **H₂1** and **Zn1**, and of the bidentate ligand DABCO. (b) Molecular modeling representations (front and side view) of the aromatic parts of **H₂1** and **Zn1**, based on NMR studies in CDCl₃.⁹ (c) Schematic representation of a possible intermolecular 'glueing' geometry of porphyrin hexamers **Zn1** + DABCO into columnar stacks; orange blocks represent intermolecularly coordinating DABCO molecules.

porphyrin trimers, hexamers, and dodecamers displayed peculiar self-assembly behaviour at surfaces. Because of their disk-like geometry and extended aromatic surfaces, and aided by their physisorption to a surface, they have the tendency to arrange themselves into well-defined and stable columnar stacks, which can form micrometer-sized or even millimeter-sized patterns.^{8,11} In several cases, we were able to manipulate these surface assemblies *via* metal–ligand coordination interactions. For example, the addition of DABCO to assemblies of metal-porphyrin hexamer **Zn1** (Fig. 1a) at a solid/liquid interface had a dramatic impact on their definition and stability.¹² Scanning tunneling microscopy (STM) studies revealed that in the absence of the ligand **Zn1** formed columnar stacks, albeit being relatively short and incoherent. After the addition of DABCO, however, extended domains of highly stable and well-defined stacks were formed, in which individual molecules of **Zn1** could be clearly resolved. This behaviour was ascribed to DABCO acting as a “supramolecular glue” (Fig. 1c). A model was proposed in which DABCO binds in between the zinc porphyrin hexamers and connects the molecules *via* bidentate coordination. Similar “glueing” of assemblies by the action of bidentate ligands was observed in the case of STM studies of the related zinc porphyrin dodecamers.¹⁰ So far, however, these studies have not been extended to self-assembly behaviour of these hexamers in solution.

Here we discuss the effect of the complexation between **Zn1** and DABCO in (deuterated) chloroform solution, by investigating the metal–ligand coordination properties with the help of UV/vis and ¹H NMR spectroscopy, and the overall size and shape of the resulting assemblies with the help of small angle neutron scattering (SANS). For comparison, also the properties of the related free base derivative **H₂1** will be described.

2. Results and discussion

2.1 Coordination of DABCO to Zn1: UV/Vis-studies

The addition of DABCO to a micromolar solution of **Zn1** in (non-deuterated) chloroform resulted in a 5 nm redshift of the Soret band from 424 to 429 nm, which is indicative of the formation of a sandwich complex with the porphyrins in a cofacial orientation (Fig. 2).⁶ Considerable redshifts were also observed in the Q-band region of the absorption spectra.

The absorbance of the new band at 429 nm increased upon the addition of DABCO, and saturation was reached after the addition of only three equivalents. These observations point at the formation of a 1:3 **Zn1**:DABCO sandwich complex. Assuming independent binding sites, the data points in Fig. 2b could be fitted to give an association constant $K_{\text{ass}} = 5.4 \times 10^6 \text{ M}^{-1}$, which is in line with the expectation for the binding strength of sandwich complexes of this ligand with zinc porphyrins.¹³ Considering the molecularly modeled conformation of the hexamer in solution, in which the six porphyrin moieties are arranged in three pairs around the benzene core (Fig. 1b),⁹ intramolecular sandwich complexes are tentatively proposed. The modeling also indicated that there is enough flexibility in the molecules, because of the presence of the oxymethylene spacers to allow such intramolecular complexation.

2.2 Coordination of DABCO to Zn1: NMR studies

In order to obtain more insight into the geometry of the complex, ¹H NMR studies were performed. The addition of DABCO to a solution of **Zn1** (1.6 mM concentration) in CDCl₃ resulted in severe broadening of the porphyrin resonances (Fig. 3b). Notably the resonances of the phenyl and alkoxy substituents at the *cis*-positions (Fig. 3a, and marked by asterisks

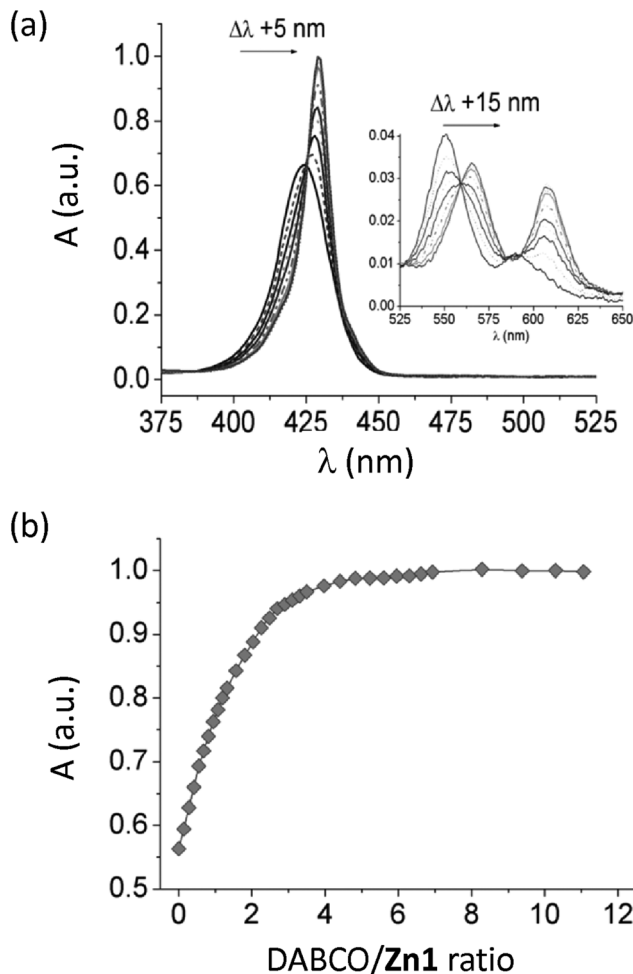


Fig. 2 (a) Changes in the UV/Vis-spectra upon the addition of DABCO to **Zn1** (0.36 μM) in chloroform (inset: magnification of the Q-band region). (b) Titration curve monitoring the change in the absorbance at 429 nm (data points derived from the spectra displayed in (a)).

in Fig. 3b) broadened and disappeared into the baseline upon the addition of 3 equivalents of DABCO. These observations are attributed to a change in conformation of the hexamer molecules. The preference of the six porphyrins in a hexamer to intramolecularly stack into three pairs of dimers (Fig. 1b and 3a), which was previously derived from molecular modeling calculations based on the strongly upfield shifted resonances of the protons of the *cis*-phenyl substituents and on intramolecular nOe contacts in solution NMR spectra,⁹ probably becomes less favorable upon the binding of DABCO. We propose that the porphyrins rearrange to form intramolecular dimers in which the porphyrins are in a cofacial orientation, with DABCO being sandwiched in between them and acting as a spacer *via* axial ligand coordination. After the addition of excess DABCO (up to 6 equivalents), some of the resonances (e.g. those of the β -pyrrole protons between 8.5 and 9 ppm) sharpened and shifted downfield again, but the other peaks in the spectra remained broad (Fig. 3b).

Considering the complexity and poor resolution of the signals of the aromatic protons of **Zn1**, we focused our attention on the strongly upfield-shifted resonances of the DABCO ligand, which were much better resolved. At the early stages of the NMR-titration, multiple resonances were observed for the DABCO methylene protons around -5 ppm, indicating the presence of sandwich-like complexes (Fig. 4a).¹⁴ The widths and upfield shifts of the observed resonances (Fig. 4b) are consistent with the presence of several intramolecular and intermolecular sandwich complexes. The sharp resonances between -4.8 and -5.5 ppm at low DABCO/**Zn1** ratios indicate that those sandwich complexes are in slow exchange with excess **Zn1**.

Up to the addition of three equivalents of DABCO per hexamer, a sharp singlet was observed at -4.86 ppm (Fig. 4a), which is attributed to the protons of the ligand in a well-defined and relatively stable sandwich complex. The large upfield shift ($\Delta\delta = -7.66$ ppm) for the DABCO resonance is

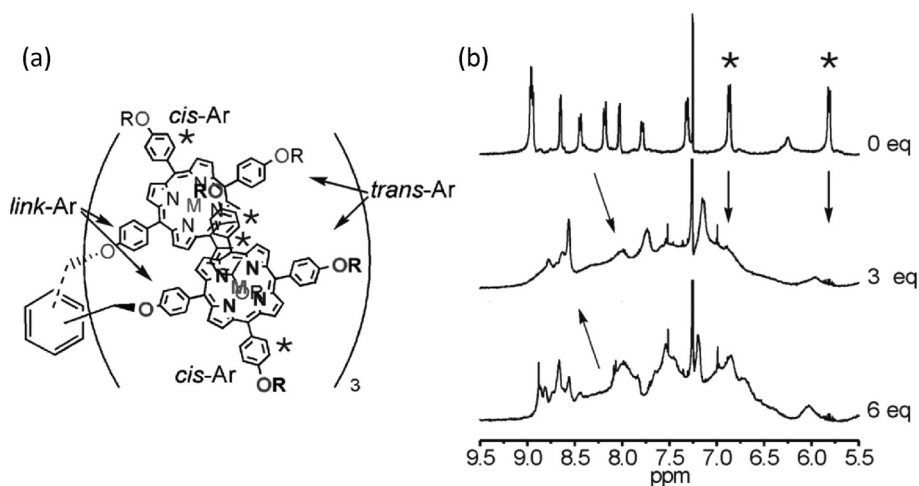


Fig. 3 (a) Definition of *cis*-, *trans*- and *link*-phenyl substituents in porphyrin hexamers. (b) Aromatic region of the ^1H NMR of titrations of **Zn1** with DABCO in CDCl_3 , demonstrating the severe broadening of the porphyrin resonances.

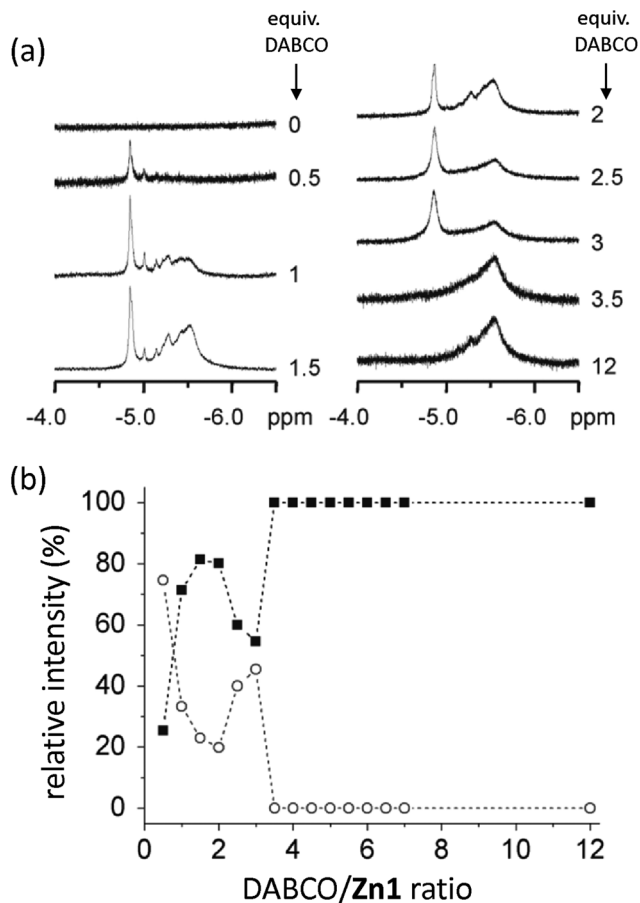


Fig. 4 (a) ^1H NMR region of the resonance of DABCO in sandwich complexes with zinc porphyrins during the NMR titration of the ligand with **Zn1** (1.6 mM) in CDCl_3 . (b) Plot of the relative intensities of the resonances at -5.55 ppm (squares) and -4.86 ppm (circles) in the NMR spectra during the titration.

consistent with a tight sandwich complex in which the two zinc porphyrin planes are oriented parallel and in close proximity.¹⁴ We propose that this resonance belongs to DABCO ligands that are intramolecularly sandwiched between the porphyrin pairs of the propeller-like geometry of **Zn1** to form a discrete 3 : 1 complex (Fig. 5b, right).

The observation of other, smaller sharp signals that were even further upfield shifted suggests that they belong to complexes in which the sandwiched DABCO molecules experience additional ring current effects, most likely as a result of the vicinity of adjacent porphyrin moieties. At low DABCO/**Zn1** ratios (0–2), it can be expected that dynamic, supramolecular complexes are formed in which DABCO is sandwiched intramolecularly, while nearby uncomplexed zinc porphyrins within the molecule stack with the sandwich complexes at either side (Fig. 5b, left and middle). At DABCO/**Zn1** ratios between 2 and 3, the possibilities of such intramolecular stacking become reduced, and the sharp, more upfield shifted resonances were no longer observed. At these ratios, the sharp singlet at -4.86 ppm, belonging to the fully occupied propeller, still remained (Fig. 5b, right).

During the titration – notably already after the addition of more than 1 equivalent of DABCO – another, rather broad resonance, which was shifted more upfield by -0.69 ppm (at -5.55 ppm), emerged and gradually increased in intensity. The very large upfield shift of $\Delta\delta = -8.35$ ppm of the DABCO proton signal is attributed to a zinc porphyrin sandwich complex that experiences significant additional ring current effects of porphyrin moieties in its vicinity. Since it seems unlikely that the intramolecular DABCO : **Zn1** complexes would self-assemble at DABCO/**Zn1** ratios of 3 or more, we propose that the resonance at -5.55 ppm belongs to sandwich complexes in which DABCO ligands bind intermolecularly (Fig. 5c). This conclusion is supported by the increase in width of the proton signal, which is consistent with an increase in molecular weight of the assembly.

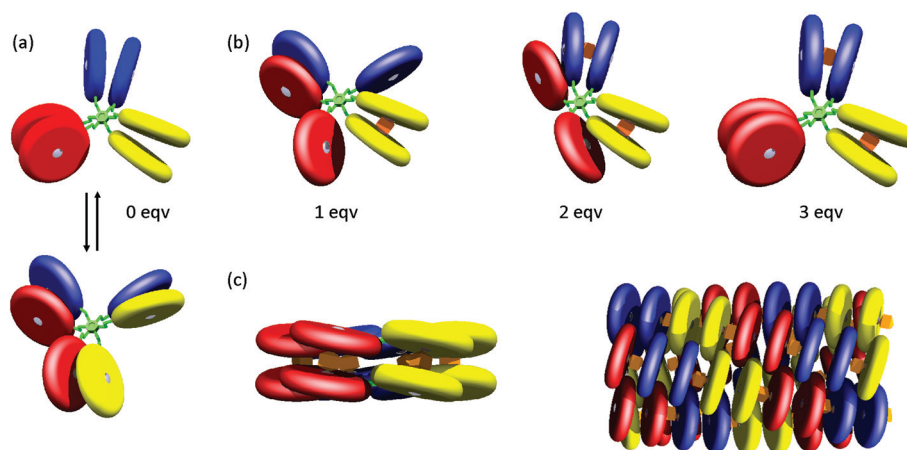


Fig. 5 Schematic representations of (a) **Zn1** molecules in the absence of DABCO; (b) several intramolecular sandwich complexes, which are proposed to be present during the ^1H NMR titration at low DABCO/**Zn1** ratios (≤ 3); and (c) intermolecular sandwich complexes (left: dimeric; right: polymeric), which are found in the presence of more than 3 equivalents of DABCO.

Beyond the addition of 3 equivalents of DABCO, a sharp transition point was observed in the titration. At this stoichiometry, the integrated areas of the two major resonances were observed to be almost equal (Fig. 4b), implying that intramolecular and intermolecular sandwich complexes were both present in comparable abundance. After the addition of more than 3 equivalents (≥ 3.5), the signal at -4.86 ppm, which was attributed to the intramolecular sandwich complex, disappeared completely and only the broad singlet at -5.55 ppm, belonging to the proposed intermolecular sandwich complexes, remained. The very abrupt disappearance of the intramolecular sandwich complex indicates that the full transition to intermolecular sandwich complexes is a highly cooperative, all-or-nothing process.^{15,16} Such outspoken behavior has been earlier reported for the formation of Anderson's ladder complexes,^{3,15} and was attributed to the combined effects of cooperativity because of the presence of multiple porphyrin binding sites, and a chelate effect because of the presence of bidentate ligands. In the present case, a dimeric sandwich complex of **Zn1** and DABCO (Fig. 5c) can be considered as a circular-shaped ladder complex, and its formation can be expected to be driven by the same factors as proposed for the previously reported ladder complexes. A unique feature of our system is, however, that larger, polymeric assemblies can be envisaged to form, in which additional π - π stacking interactions between the porphyrins and the binding of DABCO can act in synergy (Fig. 5c, right). Such oligomeric or polymeric assemblies are expected to be stable as a result of three cumulative effects: (i) π - π stacking interactions between the porphyrins, (ii) cooperativity effects as a result of the multiple binding sites for DABCO, and (iii) the chelate effect of the sandwiched ligand. In both the dimeric and polymeric intermolecular sandwich complexes, DABCO ligands are expected to fit snugly, while binding to two zinc centers simultaneously.

The huge upfield shift of $\Delta\delta = -8.35$ ppm suggests that the DABCO ligand experiences ring current effects of more porphyrins than just the two to which it coordinates, and probably also more than just the neighboring porphyrins of the sandwich complex. We therefore propose that, although a discrete dimeric ladder complex (Fig. 5c, left) is feasible, the intermolecular sandwich complex with DABCO corresponding to the observed resonance at -5.55 ppm in fact has a polymeric structure (Fig. 5c, right). The proposed polymeric assemblies are extremely stable: the resonance at -5.55 ppm remained unchanged (with respect to width and shift) even in the presence of a large excess of DABCO. Complexes in which the ligand binds in a monotopic fashion were never observed, neither in the presence of excess ligand (12 equivalents) nor after dilution (1000-fold). The reluctance of the sandwich complex to opening up clearly demonstrates very large cooperativity and chelate effects and hence a strong overall binding. Given the applied concentrations it can be estimated that K_{ass} must be larger than 10^8 M^{-1} .¹⁷ The spectroscopic studies above, however, provide only indirect information on the assembly and its nature. We therefore applied a scattering technique that is sensitive to the formed structures and allows

molecular modeling parameters to be compared, as described in the next section. In view of the high K_{ass} , the lifetime of the supramolecular interactions plays a minor role, and it is expected that the results can be interpreted assuming a static average of a dynamic system.

2.3 SANS experiments

2.3.1 Analysis of the experimental scattering profiles.

For optimum contrast, the SANS studies on the aggregation of the (non-deuterated) porphyrins were carried out in the deuterated solvent, CDCl_3 . Specific details of the theory underlying our approach to the analysis of the scattering profiles are given in the ESI.† In summary, the various regions of the scattering vector q (Fig. 6) contain information on respectively the relative dimensions of core and shell (region A), the (in our case, rodlike) shape of the aggregates (region B) and the overall radius of gyration (region C). From the scattering profile depicted in Fig. 6 the following qualitative conclusions can be drawn for the system **Zn1** + DABCO. First, the considerably enhanced forward scattering intensity (compared to other mixtures in this work, *vide infra*) indicates the presence of scattering particles with a size of the order of the inverse minimum scattering vector, q_{min} , at about 0.007 \AA^{-1} in the sample solution. The incoherent background scattering from CDCl_3 was measured separately and subtracted from that of the sample solutions. The scattering is proportional to the total amount of scattering particles; there can be many small scattering objects, or fewer but larger scattering particles, *i.e.* assemblies. Nevertheless, one will be able to distinguish the two cases by their different q -dependence, which is a function of the particle dimensions. The apparent fine structure in region A is typical for spherical or cylindrical particles. In the intermediate region B ($q \sim 0.01$), a linear part can be recognized (although it is not very pronounced), which indicates a q^{-1} behavior for this sample and is evidence for a rodlike character of the aggregates as mentioned above.¹⁸ Similar rodlike geometries of porphyrin assemblies were concluded from scatter-

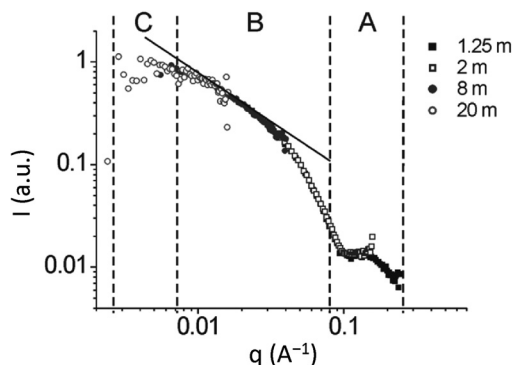


Fig. 6 Experimental scattering profile measured for **Zn1** + DABCO ($[\text{Zn1}] = 2.8 \text{ mM}$) at 4 different positions from the detector. Information about the geometry and size of the scattering object can be derived from different q -regions, denoted as A, B and C (see text).

ing studies of related porphyrin trimers reported earlier by us,¹⁹ as well as of other porphyrin compounds.²⁰

At low q , the scattering profile reaches a Guinier plateau, which indicates that the rods do not strongly interact with each other. This allows an additional estimation of the size of the particles *via* their mean volume, independent of the average length of the rods and their radii derived from the q -dependent form factor. In this work, the distribution of lengths was neglected and parameters correspond to the average over the distribution of the lengths.

Employing the Guinier expression for the calculation of the radius of gyration (eqn (6), ESI†) values of R_g ranging from $75 \pm 1 \text{ \AA}$ using data from the lowest q up to $q = 0.02$, up to $R_g = 106 \pm 14 \text{ \AA}$ with $q_{\text{max}} = 0.01$ can be found. These values correspond to average cylinder lengths of 260 \AA to 365 \AA , respectively (*via* $R_g = \sqrt{(1/12)L}$ for infinitely thin rods). The deviations can be accounted for by the relatively low signal-to-noise ratio at long detector distances (low q , see both Fig. 6 and 7) and the inaccuracy of the low q approximations if contributions of the length L and the radius R are not well separated; in this case the full description of the form factor is required, such as used

in the simulations discussed below and in the ESI.† Beside this, the estimated lengths correspond to a columnar stack of ~ 30 hexamer molecules, having a molecular weight of $\sim 250 \text{ kDa}$. The formation of columnar stacks is in line with the intermolecular coordination complexes proposed from the NMR studies in section 2.2, and from the STM studies at a solid/liquid interface previously reported by us.¹²

2.3.2 Contrast conditions for core and shell. Because the structure of the molecules in our self-assembled aggregates can be conceived as constructed from a core (the benzene ring) and an inner (porphyrin) and outer (alkyl tails) shells with different scattering length densities (SLDs) for neutrons, we considered whether our SANS data could be simulated in a way that would give us information on the dimensions of cores and shells, by analogy to our analysis of the SANS results of the RNA core and protein shell of the CCMV virus.²¹ As described in detail in the ESI,† the expected SLDs for the various regions in the self-assembling molecule were calculated on the basis of the molecular formulae, resulting in values of $1.2 \times 10^{10} \text{ cm}^{-2}$ and $-3.52 \times 10^9 \text{ cm}^{-2}$ for the core and outer shell, respectively, and values in the range $2.85\text{--}3.08 \times 10^{10} \text{ cm}^{-2}$ for the porphyrin shell, depending on the presence of metal and/or DABCO. On the basis of these results, a significant contrast would be expected between the outer shell and the solvent CDCl_3 (SLD $3.16 \times 10^{10} \text{ cm}^{-2}$); it has to be taken into account, however, that the alkyl tails do not fill this shell completely, and that the remaining space is taken up by solvent molecules, which considerably weaken the contrast. The chemically identifiable shells are not compact, neither massive nor dense. Therefore, neither the approach in which the core was considered to consist of the benzene and porphyrin, and the shell of the alkyl tails, nor that in which the benzene alone was taken as the core, and the porphyrin and alkyl regions combined to give the shell, was expected to give a result that would allow core and shell to be unambiguously distinguished. The core-shell approach was therefore abandoned, and a model assuming a homogeneous effective-averaged cylinder was adopted; the overall SLD of the porphyrin hexamer ($2.6 \times 10^{10} \text{ cm}^{-2}$) is sufficient to give contrast with CDCl_3 . In spite of this necessary simplifying approximation, the resulting parameters were observed to fit the experimental data very accurately (see next section). While detailed information on the internal construction of the rod is not obtained, these results can be considered confidently as unambiguous proof of the assembly of the disks of **Zn-1** into rodlike aggregates upon addition of DABCO, and as a good estimate of their length and radius.

2.3.3 SANS simulations and effects of dilution. Non-linear curve fitting was performed on porphyrin hexamer samples **Zn1** + DABCO (ratio $\sim 1 : 8$) and **H₂1** at different concentrations, according to the model for a homogeneous cylinder (which by the way can, in simplified form, also be applied to spheres). It involves the following set of maximally 5 variables: the contrast $(\text{SLD}_{\text{cyl}} - \text{SLD}_{\text{chloro}})^2$, ϕ , L , R and B_{gr} . The parameter L is irrelevant in the case of spheres. B_{gr} is the remaining q -independent incoherent background of the mainly hydrogenous scattering

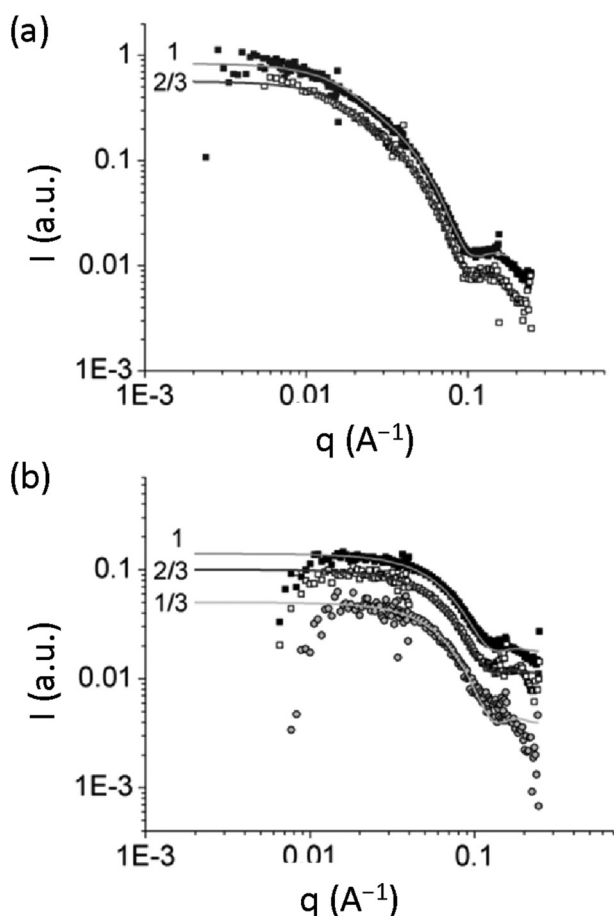


Fig. 7 SANS scattering profiles for (a) **Zn1** + DABCO (DABCO/**Zn1** ratio ~ 8), and (b) **H₂1**, at different dilutions from the starting concentration, denoted as 1, 2/3 and 1/3, respectively. The solid lines are the corresponding fits.

objects (since the incoherent level of CDCl_3 was already eliminated). Parameters $(\text{SLD}_{\text{cyl}} - \text{SLD}_{\text{chloro}})^2$ (the contrast factor) and ϕ (the volume fraction of scattering species) appear as a product and cannot be determined separately. The volume fraction of the dispersed material ϕ_{rod} can be calculated from their stoichiometry assuming that the association equilibrium of the components is shifted fully towards assembly. Since the intensity should scale with the volume fraction of species, while the contrast is a constant, the scaling of the intensity with dilution can be verified and shape changes upon concentration investigated. Knowledge of ϕ is sufficient to extract reasonable values for the contrast between the objects and the solvent.

Comparison of the scattering profiles of the different samples revealed that the scattering intensity of the **Zn1** + DABCO sample (Fig. 7a) is one order of magnitude larger than that of that of the **H₂1** sample (Fig. 7b and Table 1). Only for the **Zn1** + DABCO sample, the typical q^{-1} behaviour is observed in the curve, which indicates a 1-dimensional aggregation which separates the 2 intrinsic length scales of cylinder length and radius in a more or less pronounced way. For the **H₂1** sample, the shape of the scattering profile suggests that it is necessary and more adequate to fit the curve according to the model of homogeneous spherical particles. The q^{-1} slope and the shallow kink which appears around 0.03 \AA^{-1} where the q^{-1} behaviour stops in the case of **Zn1**, are clearly missing for **H₂1**. This assumption does not exclude stacking-aggregation of the molecules: short rodlike aggregates could still be present, but their length/radius ratio would be very close to 1 so that the length scales mix and become indistinguishable in the q^{-1} behaviour. For example, taking into account the considerable diameter of the hexamers of 62 \AA (determined from molecular modelling calculations⁹), aggregates could be present in those samples with similar length as the diameter, which would thus result in an effective overall aggregate shape of a cube or a sphere. With a thickness of the molecules of 8 \AA , such aggregates would then be built up from about 8 hexamer molecules. Although their overall hydrodynamic radius is approximately identical, the scattering intensity is expected to change accordingly at high q as the number of short distances is considerably higher in the aggregate phase than in the non-associated disklike phase. However, the data presented here allow neither justification nor rejection of this suggestion, which makes it impossible to verify whether the spherical objects are single molecules or short rodlike/effectively spherical assemblies.

Dilution of the samples turned out to not alter the shape of the curves (Fig. 7). This allows the non-trivial conclusion that the association constant K_{ass} is high and that small concentration variations hardly influence the supramolecular entity. Only the extrapolated intensity at $q = 0$ was observed to be lower (Table 1) and in line as expected from the concentration dependence of scattering. Moreover, the fitted incoherent background scattering intensity also scaled with the concentration and amounted to $\sim 10\%$ of the intensity at $q = 0$. The concentration dependence of B_{gr} highlights that the incoherent scattering is indeed the result of the protons in the scattering object, and that the corrections applied before fitting (e.g. the subtraction of chloroform) were appropriate. The volume fraction ϕ , calculated from the initial concentration of the samples was fixed and the contrast factor was refined. For the diluted samples, the resulting contrast factor was fixed to yield ϕ and B_{gr} . As can be seen in Fig. 7, the agreement is satisfactory.

The small apparent decrease in the estimated average lengths of the rods formed by **Zn1** + DABCO from 265 to 255 \AA is not considered significant in view of the fitting error ($\pm 8 \text{ \AA}$, Table 1), which suggests that the size of the aggregates does not significantly change upon dilution. Because the experimental SANS curve has not yet reached a constant value, it is possible that the observed aggregate length of $255\text{--}265 \text{ \AA}$ is in fact the maximum length that can be observed in this experiment. The number of scattering objects, expressed in the fitted volume fraction ϕ , seems to decrease as expected linearly with the dilution (see Table 1). In most cases also the scaling of the scattering intensity with dilution is linear. Since the radii of the scattering objects are unaffected by dilution by definition, the longer length may be related to the neglect of the distribution. A reason for it could be that the dilution primarily affects the shorter rods due to their lower stabilization without thereby effectively changing the average of the distribution. We note that the radii of $32\text{--}35 \text{ \AA}$ obtained from the curve fitting are in excellent agreement with those estimated by molecular modelling⁹ (31 \AA for a (metal)-hexamer). In this respect, it makes no difference whether the curve fitting is performed using the model for rods or for spheres, all results are consistent.

The observation that **H₂1** does not form extended aggregate structures is in line with expectation since at the used concentration the ^1H NMR spectrum of this compound reveal a mole-

Table 1 Dimensions of rods and spheres resulting from curve fitting

Sample	Volume fraction ϕ	Length L ($\pm 8 \text{ \AA}$)	Radius R ($\pm 1 \text{ \AA}$)	B_{gr} ($\pm 0.001 \text{ cm}^{-1}$)	Intensity at $q = 0^a$ (cm^{-1})
Zn1 + DABCO	$\phi_{\text{fixed}} = 0.030^b$	265	34	0.012	1.29
2/3 diluted	$\phi_{\text{fit}} = 0.021$	255	35	0.0073	0.86
H₂1	$\phi_{\text{fixed}} = 0.039^c$	n.a. ^d	32	0.010	0.140
2/3 diluted	$\phi_{\text{fit}} = 0.026$		33	0.011	0.094
1/3 diluted	$\phi_{\text{fit}} = 0.015$		32	0.0039	0.047

^a Extrapolated. ^b Calculated from $[\text{Zn1}] = 2.8 \text{ mM}$. Fitted SLD of the cylinder-like aggregate = $2.53 \times 10^{10} \text{ cm}^{-2}$. ^c Calculated from $[\text{H}_2\text{1}] = 3.6 \text{ mM}$. Fitted SLD of the spherical aggregate = $2.69 \times 10^{10} \text{ cm}^{-2}$. ^d Not applicable; fitted according to spherical model.

cular dissolved species⁹ (very similar to the spectrum of molecularly dissolved **Zn1** in the absence of DABCO, see Fig. 3b).

2.4 Proposed model

From the combined NMR and SANS studies an overall model for the self-assembly of **Zn1** and DABCO in solution can be derived, which complements our earlier STM studies of the complexes at a graphite surface. In the presence of a small amount of the ligand (<1 equivalent), NMR reveals that DABCO forms intramolecular coordination complexes with the zinc hexamers (Fig. 5b). In the presence of more equivalents (1–3) also the formation of intermolecular complexes starts to emerge (Fig. 5c, right), as is concluded from the broad upfield shifted signal in the NMR spectra. In the presence of more than 3 equivalents of DABCO, an abrupt and full transition to these intermolecular complexes has occurred. However, by NMR it was not possible to discriminate between discrete intermolecularly coordinated dimers (Fig. 5c, left) or polymeric stacks (Fig. 5c, right). The SANS studies of the same solutions revealed that rod-like aggregates were present, which unambiguously demonstrated that at higher DABCO–**Zn1** ratios (>3) the coordination complexes form cylindrical stacks with average lengths of at least 26 nm with the diameter of that of a single zinc hexamer molecule. We believe that the reason for the finite dimensions of the stacks is a classical example of a balance between the enthalpy and entropy factors of the self-assembly process. The aromatic parts of the hexamer macromolecules are intrinsically flexible, and in addition each of them contains 18 alkyl chains that are even more flexible. The DABCO-induced self-assembly of these molecules into stacks is favoured by a combination of enthalpic contributions coming from metal–ligand coordination, π – π stacking interactions between the porphyrin planes, and van der Waals interactions between the alkyl chains. At the same time, the self-assembly process is disfavoured by entropy loss, not only because of many hexamer and ligand molecules are brought together, but also because of the concomitant restriction in rotational/translational freedom of the flexible parts of the molecules. We believe that when the stacks grow larger, at a certain stack length it is no longer energetically favourable to add more hexamer molecules to the stack. In other words: the gain in enthalpy can no longer compensate for the loss in entropy. At that time, the stack stops growing.

3. Conclusions

The addition of DABCO to zinc porphyrin hexamer **Zn1** resulted in the formation of sandwich complexes already at micromolar concentrations, which indicates a strong binding of the ligand as result of entropically favourable intramolecular coordination and chelate effects. An NMR titration at millimolar concentrations revealed that in the presence of up to 3 equivalents of DABCO per hexamer several intramolecular and intermolecular sandwich complexes coexist. In excess of 3 equivalents of the ligand, the intramolecular com-

plexes disappear and only intermolecular complexes, in which DABCO is sandwiched between two or more **Zn1** molecules, remain. The intermolecular sandwich complexes can be considered as circular-shaped ladder complexes, which can further assemble into polymeric ones because of the cooperativity of the multiple binding sites of the hexamer in conjunction with intermolecular π – π stacking interactions and chelate effects. The combination of the above favorable effects provides the supramolecular assemblies with exceptional stability: their dissociation could not be induced in the presence of a large excess of ligand, nor upon 1000-fold dilution.

SANS-experiments provided clear evidence for rodlike aggregates of the **Zn1**–DABCO complexes in chloroform. In contrast, the metal-free porphyrin hexamer **H₂1** did not form such extended assemblies. Since the model for core–shell cylindrical aggregates could not satisfactorily describe the scattering profiles, it was simplified to that for homogeneous randomly-oriented rods with a single average SLD value for the whole aggregate. Dilution experiments showed that the length of the rods is concentration independent, while the scattering intensity scaled linearly with the concentration (*via* the volume fraction of scattering particles), a deficit possibly due to statistical uncertainties and assumptions of the monodispersity of the rod length. The curve fitting yielded for **Zn1** + DABCO an average length of the rods of 26 nm, which corresponds to an assembly of *circa* 30 porphyrin hexamer molecules.

In summary, our combined spectroscopic/scattering study on the DABCO-induced aggregation of the hexameric porphyrins revealed interesting differences between the Zn-derivative on the one hand, which formed well-defined aggregates, and the free base derivative on the other, which was not. Undoubtedly, these results will have interesting implications for the application of the Zn-hexameric porphyrins in, for example, light-harvesting materials.

4. Experimental section

4.1 Compounds

The synthesis of compounds **H₂1**⁹ and **Zn1**²² has been described in the literature. DABCO was sublimated at 60–70 °C under vacuum prior to use.

4.2 UV/vis experiments

UV/vis spectra were measured on a Varian Cary 50 Conc spectrophotometer at ambient temperature. In the UV/vis titrations, a stock solution A of **Zn1** was prepared by dissolving a known amount of the compound (approximately 1.5 mg) in 500 ml of freshly distilled chloroform. This solution was used as the solvent for the ligand molecule solution, stock B. The weighed amount of DABCO was calculated so that stock B contained the ligand in known excess with respect to **Zn1** (typically 5–10 times the expected stoichiometry of the guest/host complex). Next, 100 ml of stock B was prepared by mixing 1 ml of a stock solution 100B which is 100-fold more concentrated (with respect to ligand) with 99 ml of stock A. Aliquots of stock

B (10, 50, 100 μl) were then added to a weighed amount of approximately 1.5 ml of stock A until a total volume of 3 ml was obtained. UV/Vis-spectra were recorded immediately after each addition and the measured absorbance was plotted *versus* the calculated added equivalents of ligand.

4.3 ^1H NMR experiments

NMR-titrations were carried out on Inova400 and Bruker AMX 500 instruments. To a known amount of approximately 2 mg of **Zn1** in 500 μl of CDCl_3 small amounts (10, 25, 50 μl) of a solution of DABCO in CDCl_3 were added. The concentration of the ligand solution was calculated to contain a known number of equivalents of the “guest” per added volume (typically 0.5 or 1.0 equivalent per 10 μl). For each titration, at least 12 data points were collected by recording the NMR-spectra immediately after the addition of the ligand directly into the NMR tube.

4.4 SANS experiments

SANS experiments were performed at the KWS1 diffractometer located at the FRJ-2 Dido Reactor at Jülich, Germany. The reactor runs at 20 MW and has a D20 moderator, combined with a liquid H_2 cold source kept at 10 K. The cold white neutron beam of size $30 \times 30 \text{ mm}^2$ was monochromatized by means of a mechanical velocity selector to a wavelength λ of 7 Å with $\Delta\lambda/\lambda = 20\%$. Hellma Quartz cuvettes of path lengths 1 mm holding the sample solutions were positioned at preset distances (1.25; 2, 8 or 20 m) from the detector in the automatic sample changer. These distances provide the full scattering angle range and overlap nicely which avoids systematic errors due to different counting statistics. The beam was collimated with respectively 2, 2, 8 and 20 m to a sample aperture of $10 \times 10 \text{ mm}^2$ to achieve maximum possible flux at the sample. The 2D-detector acquired the scattering at the different positions during 10, 15, 85 and 140 min, respectively. The measuring time was increased going further away from the sample because of the poorer signal-to-noise ratio at smaller angles.

The detection of the scattered neutrons was 2-dimensional in 128×128 channels of each $5.2 \times 5.2 \text{ mm}^2$. The detector was of the photomultiplier type, which has the advantage over gas detectors in the sense that the dynamical range of intensities is high and no damage due to local high counting rates can be expected. Its deadtime τ is 4.5 microseconds, allowing integral counting rates of approximately 20 000 counts per second. The sensitivity of the detector channels was determined from the measurement of a flat-scattering incoherent sample, *i.e.* Plexiglas or H_2O and every cell was corrected for the detector's sensitivity pixelwise. The measured neutrons in each configuration were put on to absolute intensity scale (cm^{-1}), which allows comparison with theoretical calculations and with different instruments at other neutron sources. The corrected intensities were obtained after appropriate subtraction of empty cell scattering, background noise from stray neutrons and gammas and dark current noise from the electronics. Possible deadtime effects were accounted for in the cali-

bration. Absolute macroscopic differential cross-sections, denoted as intensities I in the text, were obtained after calibrating with a 1.5 mm thick secondary standard of Plexiglas which had been calibrated to Vanadium before.

Measuring the standard Plexiglas at identical collimation conditions as the sample, *i.e.* at the same flux conditions but at a shorter distance, and then scaling the intensity for the correct solid angle leads to an automatic overlap of the different camera distances. Instead of dividing the intensity by the flat intensity of the calibrant, the average intensity of Plexiglas is used together with a sensitivity correction per channel (ϵ_{ij}). This has the advantage of decoupling calibration and sensitivity corrections. All above corrections are performed in 2D (128×128) pixelwise after which a radial averaging of the data – *i.e.* gathering of intensities at the same scattering vector – reduces the full 2D data to I vs. q data.

The transmissions were measured *in situ* from a neutron monitor inside the beamstop and yielded on the average $T = 71\%$. The absolute incoherent intensity of the solvent CDCl_3 acts like an additional background and was determined from the q -range between 0.03 and 0.26 \AA^{-1} . This yielded an incoherent q -independent background contribution of $(0.030 \pm 0.001) \text{ cm}^{-1}$. This average value was subtracted instead of the respective data at all q -values for statistical reasons. This low intensity – compare to water: 1 cm^{-1} – is highly influenced by varying backgrounds and experimental conditions and especially the low q data are obtained with large error bars for which the low signal-to-noise ratio is responsible. Parasitic scattering around the beam stop from the neutron transmission monitor cannot be avoided either and may lead to somewhat exaggerated subtractions at low q . The transmissions are accurate to within 1% and determined typically in the 8 m distance from an *in situ* measurement of the transmitted beam in the center of the beam stop. Scattering lengths for the elements were obtained from tables on the basis of bruto formula and bulk densities.

The recorded scattering intensity I was plotted as a function of the scattering vector q on a log-log scale. The scattering vector q is related to the scattering angle θ via $q = 4\pi/\lambda \cdot \sin(\theta/2)$. With this scattering vector range and the neutron wavelength $\lambda = 7 \text{ \AA}$ (with a wavelength spread $\Delta\lambda/\lambda = 0.20$) distances of $2\pi/q$ between 25 Å and 3000 Å are within reach of investigation. The resulting scattering profiles were analyzed qualitatively immediately after collection of the data and curve fitting was performed later to obtain more quantitative information.

Conflicts of interest

There are no conflicts to declare.

Acknowledgements

This work was supported by the Dutch National Research School Combination Catalysis (NRSC-C) and a grant from the

Dutch Ministry of Education, Culture and Science (Gravity program 024.001.035). R. J. M. N. acknowledges support from the European Research Council (ERC Advanced grant ENCOPOL 740295). The Helmholtz Society (Germany) is acknowledged for the provision of beam time and support at the Forschungszentrum Jülich; this research project has been supported by the European Commission under the 6th Framework Programme through the Key Action: Strengthening the European Research Area, Research Infrastructures, contract no: RII3-CT-2003-505925.

References

- C. B. Kc and F. D'Souza, *Coord. Chem. Rev.*, 2016, **322**, 104; S. Chen, P. Slattum, C. Wang and L. Zang, *Chem. Rev.*, 2015, **115**, 11967; Q. Yan, Z. Luo, K. Cai, Y. Ma and D. Zhao, *Chem. Soc. Rev.*, 2014, **12**, 4199; F. Würthner, T. E. Kaiser and C. R. Saha-Möller, *Angew. Chem., Int. Ed.*, 2011, **50**, 3376; J. A. A. W. Elemans, R. van Hameren, R. J. M. Nolte and A. E. Rowan, *Adv. Mater.*, 2006, **18**, 1251.
- G. McDermott, S. M. Prince, A. A. Freer, A. M. Hawthornthwaite-Lawless, M. Z. Papiz, R. J. Cogdell and N. W. Isaacs, *Nature*, 1995, **374**, 517; T. Pullerits and V. Sundström, *Acc. Chem. Res.*, 1996, **29**, 381; S. Bahatyrova, R. N. Frese, C. A. Siebert, J. D. Olsen, K. O. van der Werf, R. van Grondelle, R. A. Niederman, P. A. Bullough, C. Otto and C. N. Hunter, *Nature*, 2004, **430**, 1058; S. Scheuring, J. Seguin, S. Marco, D. Levy, B. Robert and J. L. Rigaud, *Proc. Natl. Acad. Sci. U. S. A.*, 2003, **100**, 1690; L.-J. Yu, M. Suga, Z.-Y. Wang-Otomo and J.-R. Shen, *Nature*, 2018, **556**, 209.
- H. L. Anderson, *Inorg. Chem.*, 1994, **33**, 972; P. N. Taylor and H. L. Anderson, *J. Am. Chem. Soc.*, 1999, **121**, 11538; C. A. Hunter and H. L. Anderson, *Angew. Chem., Int. Ed.*, 2009, **48**, 7488.
- S. J. Lee, S.-H. Cho, K. L. Mulfort, D. M. Tiede, J. T. Hupp and S. T. Nguyen, *J. Am. Chem. Soc.*, 2008, **130**, 16828; L. Flamigni, B. Ventura, A. I. Oliva and P. Ballester, *Chem. – Eur. J.*, 2008, **14**, 4214; P. Ballester, M. Claudel, S. Durot, L. Kocher, L. Schoepff and V. Heitz, *Chem. – Eur. J.*, 2015, **21**, 15339; X. Wang, S. S. Nurttilla, W. I. Dzik, R. Becker, J. Rodgers and J. N. H. Reek, *Chem. – Eur. J.*, 2017, **23**, 14769.
- B. Zhu, H. Chen, W. Lin, Y. Ye, J. Wu and S. Li, *J. Am. Chem. Soc.*, 2014, **136**, 15126; M. C. O'Sullivan, J. K. Sprafke, D. V. Kondratuk, C. Rinfray, T. D. W. Claridge, A. Saywell, M. O. Blunt, J. N. O'Shea, P. H. Beton, M. Malfois and H. L. Anderson, *Nature*, 2011, **469**, 72.
- A. Rana, P. K. Biswas and M. Schmittel, *Dalton Trans.*, 2017, **46**, 9491; S. Cantekin, A. J. Markvoort, J. A. A. W. Elemans, A. E. Rowan and R. J. M. Nolte, *J. Am. Chem. Soc.*, 2015, **137**, 3915; B. R. Danger, K. Bedient, M. Maiti, I. J. Burgess and R. P. Steer, *J. Phys. Chem. A*, 2010, **114**, 10960; P. Ballester, A. Costa, A. M. Castilla, P. M. Deyà, A. Frontera, R. M. Gomila and C. A. Hunter, *Chem. – Eur. J.*, 2005, **11**, 2196; P. Thordarson, R. G. E. Coumans, J. A. A. W. Elemans, P. J. Thomassen, J. Visser, A. E. Rowan and R. J. M. Nolte, *Angew. Chem., Int. Ed.*, 2004, **43**, 4755.
- C. Oliveras-González, F. Di Meo, A. González-Campo, D. Beljonne, P. Norman, M. Simón-Sorbed, M. Linares and D. B. Amabilino, *J. Am. Chem. Soc.*, 2015, **137**, 15795; S. A. L. Rousseaux, J. Q. Gong, R. Haver, B. Odell, T. D. W. Claridge, L. M. Herz and H. L. Anderson, *J. Am. Chem. Soc.*, 2015, **137**, 12713; A. Camara-Campos, C. A. Hunter and S. Tomas, *Proc. Natl. Acad. Sci. U. S. A.*, 2006, **103**, 3034.
- R. van Hameren, P. Schön, A. M. van Buul, J. Hoogboom, S. V. Lazarenko, J. W. Gerritsen, H. Engelkamp, P. C. M. Christianen, H. A. Heus, J. C. Maan, Th. Rasing, S. Speller, A. E. Rowan, J. A. A. W. Elemans and R. J. M. Nolte, *Science*, 2006, **314**, 1433; R. van Hameren, A. M. van Buul, M. A. Castriciano, V. Villari, N. Micali, P. Schön, S. Speller, L. Monsù Scolaro, A. E. Rowan, J. A. A. W. Elemans and R. J. M. Nolte, *Nano Lett.*, 2008, **8**, 253; N. Veling, R. van Hameren, A. M. van Buul, A. E. Rowan, R. J. M. Nolte and J. A. A. W. Elemans, *Chem. Commun.*, 2012, **48**, 4371.
- H. A. M. Biemans, A. E. Rowan, A. Verhoeven, P. Vanoppen, L. Latterini, J. Foekema, A. P. H. J. Schenning, E. W. Meijer, F. C. de Schryver and R. J. M. Nolte, *J. Am. Chem. Soc.*, 1998, **120**, 11054.
- M. C. Lensen, S. J. T. van Dingenen, J. A. A. W. Elemans, H. P. Dijkstra, G. P. M. van Klink, G. van Koten, J. W. Gerritsen, S. Speller, R. J. M. Nolte and A. E. Rowan, *Chem. Commun.*, 2004, 762; M. C. Lensen, J. A. A. W. Elemans, S. J. T. van Dingenen, J. W. Gerritsen, S. Speller, A. E. Rowan and R. J. M. Nolte, *Chem. – Eur. J.*, 2007, **13**, 7948.
- M. C. Lensen, K. Takazawa, J. A. A. W. Elemans, C. R. L. P. N. Jeukens, P. C. M. Christianen, J. C. Maan, A. E. Rowan and R. J. M. Nolte, *Chem. – Eur. J.*, 2004, **10**, 831; C. R. L. P. N. Jeukens, M. C. Lensen, F. J. P. Wijnen, J. A. A. W. Elemans, P. C. M. Christianen, A. E. Rowan, J. W. Gerritsen, R. J. M. Nolte and J. C. Maan, *Nano Lett.*, 2004, **4**, 1401.
- J. A. A. W. Elemans, M. C. Lensen, J. W. Gerritsen, H. van Kempen, S. Speller, R. J. M. Nolte and A. E. Rowan, *Adv. Mater.*, 2003, **15**, 2070.
- H. L. Anderson, C. A. Hunter, M. N. Meah and J. K. M. Sanders, *J. Am. Chem. Soc.*, 1990, **112**, 5780; E. L. Puranen, M. E. Stapelbroek-Mollmann, E. Vuorimaa, N. Tkachenko, A. Y. Tauber, P. H. Hynninen and H. Lemmetyinen, *J. Photochem. Photobiol., A*, 2000, **136**, 179–184.
- P. Mondal and S. P. Rath, *Chem. – Eur. J.*, 2016, **22**, 5607; R. B. Murphy, D.-T. Pham, S. F. Lincoln and M. R. Johnston, *Eur. J. Org. Chem.*, 2013, 2985.
- P. N. Taylor and H. L. Anderson, *J. Am. Chem. Soc.*, 1999, **121**, 11538.
- G. Ercolani, *J. Am. Chem. Soc.*, 2003, **125**, 16097.

- 17 A. Vidal-Ferran, Z. Clyde-Watson, N. Bampos and J. K. M. Sanders, *J. Org. Chem.*, 1997, **62**, 240.
- 18 M. Ragnetti and R. Oberthür, *Colloid Polym. Sci.*, 1986, **264**, 32; P. Terech and A. Coutin, *Langmuir*, 1999, **15**, 5513.
- 19 R. van Hameren, A. M. van Buul, D. Visser, R. K. Heenan, S. M. King, A. E. Rowan, R. J. M. Nolte, W. Pyckhout-Hintzen, J. A. A. W. Elemans and M. C. Feiters, *Soft Matter*, 2014, **10**, 9688.
- 20 V. V. Roznyatovskiy, R. Carmieli, S. M. Dyar, K. E. Brown and M. R. Wasielewski, *Angew. Chem., Int. Ed.*, 2014, **53**, 3457; F. Helmich, C. C. Lee, M. M. L. Nieuwenhuizen, J. C. Gielen, P. C. M. Christianen, A. Larsen, G. Fytas, P. E. L. G. Leclère, A. P. H. J. Schenning and E. W. Meijer, *Angew. Chem., Int. Ed.*, 2010, **49**, 3939; P. Terech, C. Scherer, B. Demé and R. Ramasseul, *Langmuir*, 2003, **19**, 10641.
- 21 M. Comellas-Aragonès, F. D. Sikkema, G. Delaittre, A. E. Terry, S. M. King, D. Visser, R. K. Heenan, R. J. M. Nolte, J. J. L. M. Cornelissen and M. C. Feiters, *Soft Matter*, 2011, **7**, 11380.
- 22 J. Foekema, A. P. H. J. Schenning, D. M. Vriezema, F. B. G. Benneker, K. Nørgaard, J. K. M. Kroon, T. Bjørnholm, M. C. Feiters, A. E. Rowan and R. J. M. Nolte, *J. Phys. Org. Chem.*, 2001, **14**, 501.